Research Article

Muhammad Naveed*, Noor ul Ain, Tariq Aziz*, Ayesha Saleem, Muhammad Aqib Shabbir, Ayaz Ali Khan, Thamer H. Albekairi

# Integrated track of nano-informatics coupling with the enrichment concept in developing a novel nanoparticle targeting ERK protein in *Naegleria fowleri*

https://doi.org/10.1515/chem-2023-0198
received November 22, 2023; accepted January 23, 2024

**Abstract:** *Naegleria fowleri* is a free-living amoeba that causes primary amoebic meningoencephalitis. Despite combination drug therapies, *N. fowleri* is not sensitive to current drug therapies, contributing to the pathogen's mortality rate of 98%. To enable rational drug designing, this study has proposed an integrated track of nanotechnology coupling with the enrichment concept. In the current study, zinc oxide nanoparticles (ZNP) were screened against ERK protein, which is responsible for the production of pro-inflammatory cytokines that cause brain disturbance in *N. fowleri infection.* Furthermore, an enrichment analysis has been executed to increase the efficiency of the ZNP through the addition of two amines and one chlorine group. The computational prediction of zeta potential, cytotoxicity, organ toxicity, calculations of binding free energy, and ADMET analysis shows that it is stable and possesses no toxic effect. Amine + chlorine enriched ZNP resulted in a binding energy of −7.8 kcal/mol, a zeta potential reliability of −40 mV, a cytotoxicity of −0.0002, inactive against all the targeted organ models, ADMET profiling shows a molecular weight of 320.54 g/mol, a lipophilicity of −0.99, high water solubility, and good gastrointestinal tract absorption. This proposed invention represents the future work for in vitro in combating this devastating disease toward a reliable therapeutic target with drugs that specifically aimed to inhibit the infection.

**Keywords:** primary amoebic meningoencephalitis, non-vehicle, nanoparticles, blood–brain barrier

## 1 Introduction

*Naegleria fowleri* infection, also known as "brain-eating amoeba," causes severe brain infection known as primary amoebic meningoencephalitis (PAM). In 1965, the first case of amoebic infection was reported by Fowler and Carter from Australia [1]. Symptoms mainly comprise stiffness of the neck, high fever, seizures, disturbed mental status, headache, and coma, eventually leading to death. The fertility rate of PAM is more than 98% with hundreds of cases worldwide [2]. *N. fowleri* is found in freshwater and soil all over the world but is mainly present in warm water thriving in soil and freshwater with temperatures up to 46°C (115°F). There has been an increase in the prevalence of PAM since 2000 worldwide, and it is often linked to activities such as diving and swimming in water with high temperature [3]. The clinical symptoms of PAM are non-specific; hence, the diagnosis often occurs after the patients have died. Due to a lack of awareness, poor prognosis, and lack of global distribution of knowledge about risk factors and public health issues, amoebic meningoencephalitis cases are often misreported and underrecognized especially in developing countries [4]. Despite late diagnosis, current treatment therapies were based on a combination of drugs such as intravenous amphotericin B combined with azole antifungal, miconazole, ornidazole,

*** Corresponding author: Muhammad Naveed,** Department of Biotechnology, Faculty of Life Sciences, University of Central Punjab, Lahore 54590, Pakistan, e-mail: Naveed.quaidian@gmail.com
*** Corresponding author: Tariq Aziz,** Department of Agriculture, University of Ioannina, Arta 47100, Greece, e-mail: iwockd@gmail.com
**Noor ul Ain**, **Ayesha Saleem**, **Muhammad Aqib Shabbir:** Department of Biotechnology, Faculty of Life Sciences, University of Central Punjab, Lahore 54590, Pakistan
**Ayaz Ali Khan:** Department of Biotechnology, University of Malakand Chakdara, Chakdara, Pakistan
**Thamer H. Albekairi:** Department of Pharmacology and Toxicology, College of Pharmacy, King Saud University, P.O. Box 2455, Riyadh, 11451, Saudi Arabia

miltefosine, trifluoperazine, ceftriaxone, artesunate, dexamethasone, chloramphenicol, pentamidine, sulfadiazine, artesunate, fluconazole, ketoconazole, itraconazole, and rifampin. Miltefosine added to hypothermia in recent cases resulted in patients' survival [5,6]. Nevertheless, these antibiotics have severe side effects such as mental issues and nephrotoxicity. Moreover, administration intravenously causes poor absorption of drugs and penetration of the drug into the CNS due to the highly selective permeability of the blood–brain barrier (BBB) [7].

The pro-inflammatory cytokines namely responsive neurotransmission, Interleukins-6, tumor necrosis factor-alpha, reactive oxygen species (ROS) and Interleukins-1β were produced through the activation of the microglia cells. Excessive production of neurotoxic cytokines causes significant damage to the CNS and destruction of the brain cells [8]. *N. fowleri* activates the extracellular-signal-regulated kinase (ERK), c-Jun N-terminal kinase (JNK), and p38 mitogen-activated protein kinase pathways in response to extracellular signals, producing cytokines [9]. However, the activation of these cytokines is thought to be detrimental as it may lead to the destruction of brain tissue through an immunopathological process. This is because the release of cytokines can further weaken the BBB and trigger hyperinflammation of the immune cells from the non-neural areas [10]. Therefore, regulating the expression of these inflammatory cytokines is crucial to prevent further damage to the CNS caused by *N. fowleri* [11]. Different innovative methods have been utilizing nanoparticles that are proposed to increase permeability across the BBB, which causes an increase in the treatment efficacy of the amoebic brain infection [12]. Many types of research have shown nanotechnology for the advancement of drug delivery against PAM. Furthermore, nanovesicles have enhanced permeability, high loading capacity, and the capability of encapsulating multiple agents in a single carrier, all of which contribute to passive and active parasite targeting [13].

PAMs are one of the central nervous malignities hastened in humans exhibiting considerable mortality rate disparity. Besides the current treatment, nanotechnology could be used as a drug delivery vehicle that targets the cell surface receptors selectively [14]. The main purpose of the current study was to perform functional group optimization-based drug designing against *N. fowleri* infection based on homology modeling. The protein of ERK was selected as a target and zinc oxide nanoparticles (ZNP) were taken as a ligand. The screening of nanoparticles, functional group optimization, and ADMET analysis have been performed. This study provides a therapeutic approach for the treatment of *N. fowleri* infection.

# 2 Material and methodology

## 2.1 ERK protein 3D structure prediction

The protein structure of ERK was retrieved from the Protein Data Bank (PDB) (http://www.rcsb.org/pdb/). This is the database of the three-dimensional structure of large biomolecules such as proteins. It is key in the areas of structural biology such as structural genomics [15].

## 2.2 Specification of binding pockets

The prediction of the binding pockets of the protein was assessed through the COACH server (https://zhanggroup.org/COACH/) for an insight into the interaction with ligands. COACH server is utilized to predict the protein–ligand binding sites. These binding sites' prediction is carried out by two comparative approaches, S-SITE and TM-SITE. These approaches recognize the templates for the binding of the ligand through BioLiP protein function database (https://zhanggroup.org/BioLiP/). An interaction database is semi-manually curated for high-quality, biologically relevant protein–ligand interactions [16].

## 2.3 Nanoparticle's structure recoveries

ZNP were selected and retrieved from the PubChem database (https://pubchem.ncbi.nlm.nih.gov). It is a database that gives knowledge of chemical compounds and their biological activities [17].

## 2.4 Structure-based virtual screening

PyRx program was used for molecular screening of the library of compounds as the engine for molecular docking. Different nanoparticles that can act as a ligand were assessed for the inhibition of the amoebic infection by *N. fowleri* [18].

## 2.5 Post-refining analysis for screening

Post-refining analysis of the ZNP was done by MMGBSA software. It is a high-throughput validation method to

validate whether the method that is used for screening is accurate or if there might be some inactive compounds that were not screened or detected through the screening method [19].

## 2.6 Amine + chlorine enrichment analysis

Enrichment of amine + chlorine was performed by using the FROGS tool (http://frogs.toulouse.inra.fr/). FROGS is galaxy supported pipeline that is designed to analyze data sets and produce Operation Taxonomic Units of amplicon sequences and their taxonomic affiliations. In the best-screened ZNP, two amine groups and one chlorine group were introduced as the amine group was reported in the literature of the ZNP through FTIR analysis and chlorine was the strong group among halogens [20]. The docking analysis was performed through AutoDock Vina to check the efficiency of the amine + chlorine enriched ZNP (A + C enriched ZnO NP).

## 2.7 Prediction of interacting forces

Interaction forces and their bonds were predicted by using the web server protein–ligand interacting profiler (PLIP). PLIP gives the interactions, type of forces, atoms, and bond length present in the complex. Interaction forces can be predicted by calculating the bond length of the interacting bond through some visualization software [21].

## 2.8 Calculation of binding free energy

The prediction of binding energy was calculated through the g MMPBSA script. This method determines the electrostatic force, molecular mechanics free energy, and van der Walls interactions. The free energy of solvations such as polar and non-polar interactions was also accessed through this method. To calculate the energy terms, more than 70 shots were used at intervals from the molecular dynamic simulations. For the prediction of binding energies, the average of these energies was taken. The following equation was used to predict the binding free energy between the protein and ligand [22].

$$\Delta G_{\text{binding}} = \Delta G_{\text{A+C enriched ZnO NP-ERK}} - (G_{\text{ERK}} + G_{\text{A+C enriched ZnO NP-ERK}})$$

$$\text{Gx} = |\langle \text{EMM} \rangle - \text{TS} + |\langle \text{G}_{\text{solvation}} \rangle$$

$$\text{EMM} = E_{\text{bonded}} + E_{\text{non-bonded}} = E_{\text{bonded}} + (E\text{vdW} + E_{\text{elec}})$$

$$G_{\text{solvation}} = G_{\text{polar}} + G_{\text{non-polar}}$$

$$G_{\text{non-polar}} = \gamma \text{SASA} + b$$

Here, $G_{\text{ERK}}$ represents the free binding energy of the ERK protein and $G_{\text{A+C enriched ZnO NP-ERK}}$ free binding energy of the complex. Whereas EMM shows the vacuum molecular mechanic of potential energy, $G_{\text{A+C enriched ZnO NP}}$ is the free binding energy of the ligand, TS shows the entropic contribution of the ligand into the free binding energy, S represents the entropy, and $T$ is the temperature of the energy. The free energy of solvation is the $G_{\text{solvation}}$ which comprises both the polar and non-polar parts. The solvent-accessible surface area is represented by SASA, γ represents the coefficient of the surface tension, and the fitting constant is $b$.

## 2.9 Prediction of zeta potential

Among the critical properties of the nanoparticle was zeta potential. It provides the estimation of electrostatic stability and surface charge, therefore affecting the tendency of nanoparticles to make agglomerates and further interact with the cellular membrane. The zeta potential of A + C enriched ZnO NP is calculated from PhysChem NanoXtract (http://enaloscloud.novamechanics.com/EnalosWebApps/NanoXtract/). It utilizes the nanodiscriptors from the transmission electron microscopy (TEM) images to predict the zeta potential, behavior of nanoparticles, and their biological role. Nanomaterial TEM images are used to predict the zeta potential of the model based on the nearest neighbor [23].

## 2.10 Cytotoxicity prediction

The cytotoxicity prediction of A + C enriched ZnO NP was done through the Cytotoxicity tool (https://cellviability.-cloud.nanosolveit.eu/) from the NanoSolveIT database. It predicts the cytotoxicity of A + C enriched ZnO NP to the cell lines of murine myeloid (RAW 264.7) and to human bronchial epithelial (BEAS-2B) by using the only single parameter of % cell viability of lactate dehydrogenase and adenosine triphosphate assays. It is based on the selected molecular, physiochemical, and atomistic descriptors [24].

### 2.11 Organ toxicity evaluation

The toxicity prediction of the ZNP was evaluated through the Protox II tool (http://tox.charite.de/protox_II). It takes the 2D structure of the compounds as an input and predicts the A + C enriched ZnO NP toxicity profiles for 33 models with overall toxicity radar and confidence scores along with similar targets with known toxicity profiles [25].

### 2.12 Drug-likeness and bioactivity score

Drug-like characteristics of the drug candidate were examined by using the Molinspiration tool. Different parameters were predicted by using the Molinspiration tool such as molecular polar surface area (PSA), log *P*, range of atoms, range of rotatable bonds, nuclear receptors, ion channel modulator, and Lipinski's rule violations of the A + C enriched ZnO NP [26].

### 2.13 ADMET analysis

The ADMET analysis of A + C enriched ZnO NP was done through admetSAR (http://www.admetexp.org). It is an online tool for the prediction of ADMET properties. It contains 27 predictive models and has been widely used in pharmaceutical and chemical fields. It determines the compound's absorption, distribution, metabolism, excretion, and toxicity [27].

### 2.14 Molecular dynamic simulations

The molecular dynamic simulation was used for the analysis of docked structures by modifying the structure's force field concerning different time intervals. Molecular dynamic simulations were done by using the iMods server. It gives information about the behavior of the protein when it binds with the ligand and it also validates the interaction analysis of the ERK protein with the A + C enriched ZnO NP [28].

## 3 Results

### 3.1 ERK protein 3D structure prediction

The 3D structure of the targeted protein was retrieved through the ID mapping ERK (PDB ID: 5UMO). It consists of 364 amino acids with one chain A that starts with histidine (H) and ends at serine (S). Figure 1 shows the 3D structure of the ERK protein.

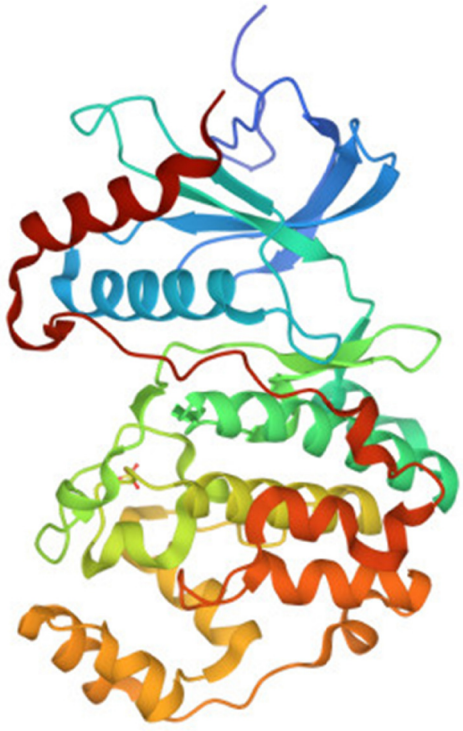

**Figure 1:** 3D structure of the ERK protein.

### 3.2 Specification of binding pockets

COACH analysis was used for the identification of binding pockets and active sites of the protein. The *C*-score is 1.00,

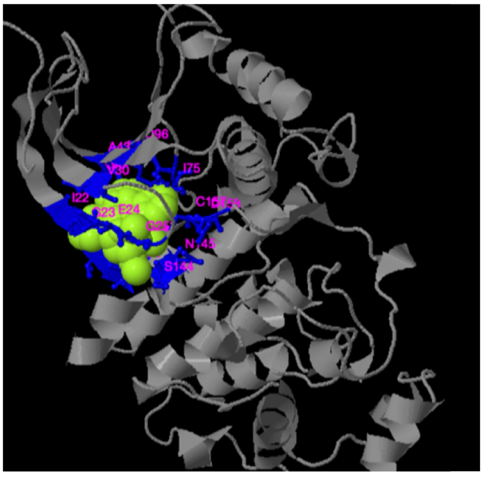


**Figure 2:** Identification of binding pockets of ERK protein using TM-SITE results. The blue color region indicates the pocket residues and the purple color indicates the name of the residues.

PDB ID: 3mj2A, ligand name MJG, and consensus binding residues are 20, 22, 23, 24, 25, 30, 43, 45, 96, 97, 98, 99, 100, 101, 102, 144, 145, 147, 157 and 158, respectively.

The TM-SITE results show a *C*-score of 0.57 with the size of the cluster being 327. The predicted binding site residues for ligand 2CV are 22, 23, 24, 25, 30, 43, 45, 75, 96, 97, 98, 99, 101, 102, 144, 145, 147, 157, and 158 as seen in Figure 2.

The S-SITE results show a *C*-score of 0.09, with a size of cluster 2, where a cluster size is the number of clusters in a template. The predicted ligands are ZN and MAN. Predicted binding site residues for ligand MAN are 22, 23, 24, 25, 27, 28, 30, 43, 45, 62, 66, 75, 94, 96, 97, 98, 99, 100, 101, 102, 105, 144, 145, 147, 157, 158, and 159 as shown in Figure 3.

## 3.3 Nanoparticle's structure recoveries

The 3D structure of ZNP was taken from the PubChem database with the PubChem ID 24424, 10290809, and 11831558 as shown in Figure 4.

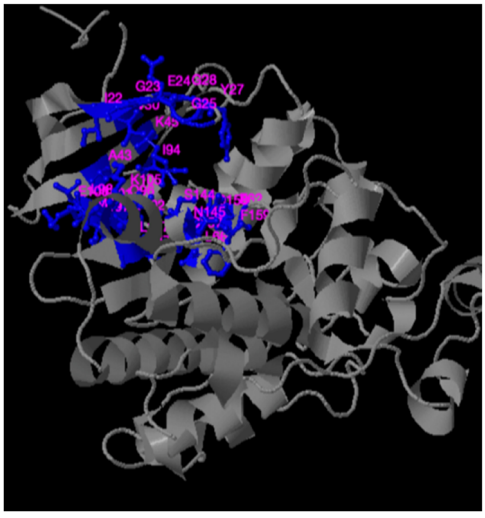


**Figure 3:** Identification of binding pockets of ERK protein using S-SITE. The blue color region indicates the pocket residues and the purple color indicates the name of the residues.

## 3.4 Structure-based virtual screening

The compounds that were retrieved through PubChem were screened against ERK protein through PyRx. The analysis revealed that zinc oxide (10290809) nanoparticle shows high docking energy −2.3 kcal/mol followed by 24424 (−1.6) and 11831558, which is −1.3.

## 3.5 Post-refining analysis for screening

The results of post-refining analysis from the MMPBSA method validate that there was only one compound that is active as shown by the results that the rest of the compounds were inactive or semi-active. Table 1 shows the results of the comparative analysis of the docking scores from the MMGBSA and PyRx.

## 3.6 Amine + chlorine enrichment analysis

The addition of two amine groups and one chlorine group results in an increase in the efficiency of the nanoparticles and it enhances the neurotransmission as docking analysis shows an increase of the binding energy to −7.8 kcal/mol. It shows that this enrichment accelerates the drug efficiency of the compounds against the brain-eating amoeba as shown in Figure 5.

**Table 1:** The comparative results of the compound docking score from the MMGBSA and PyRx database

| Nanoparticle | PyRx docking score (kcal/mol) | MMGBSA docking score (kcal/mol) |
|---|---|---|
| 10290809 | −2.3 | −78 |
| 24424 | −1.6 | −56 |
| 11831558 | −1.3 | −45 |

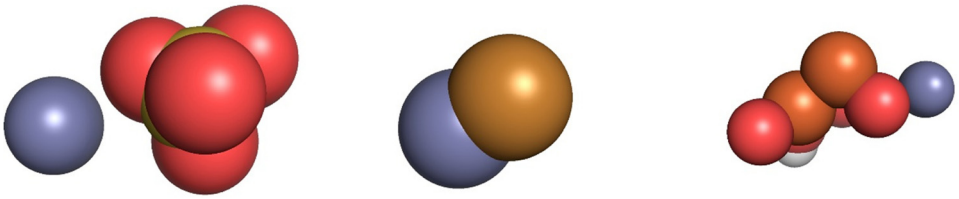

(a) (b) (c)

**Figure 4:** The 3D structures of the ZNP. (a) 24424, (b) 10290809, and 11831558.

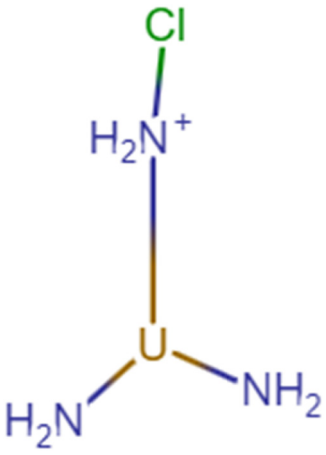


**Figure 5:** The 3D structure of the A + C ZnO NP.

## 3.7 Prediction of interacting forces

PLIP, which is an online server, was applied to predict the interaction forces of the nanoparticle complex with ERK protein. There are two interactions, that were predicted in the docked complex. For the hydrogen bond, the distance between residues is usually 2.7–3.3 Å and for the hydrophobic interaction (van der Waals forces) the carbon-to-carbon distance is usually 3.3–4 Å as shown in Figure 6 and Table 2.

**Table 2:** Residues and their interacting bonds predicted by PLIP

| Sr. no | Residues | Amino acid | Distance | Interaction force |
|---|---|---|---|---|
| 1 | 189A | ARG | 4 | van der Waals force |
| 2 | 192A | ARG | 3.99 | van der Waals force |

## 3.8 Calculation of binding free energy

The prediction of binding free energy results showed that the electrostatic force of interaction has dominated the binding free energy with a 70% percentage in contrast to the force of van der Walls interactions with a percentage of contribution of 12% as depicted in Table 3.

## 3.9 Prediction of zeta potential

The prediction of zeta potential analysis shows a value of −40 mV, meaning that the A + C enriched ZnO NP is stable and reliable (Table 4).

## 3.10 Cytotoxicity prediction

The cytotoxic prediction of A + C ZnO NP shows a value of 0.0002 against cancerous cell lines which means that it

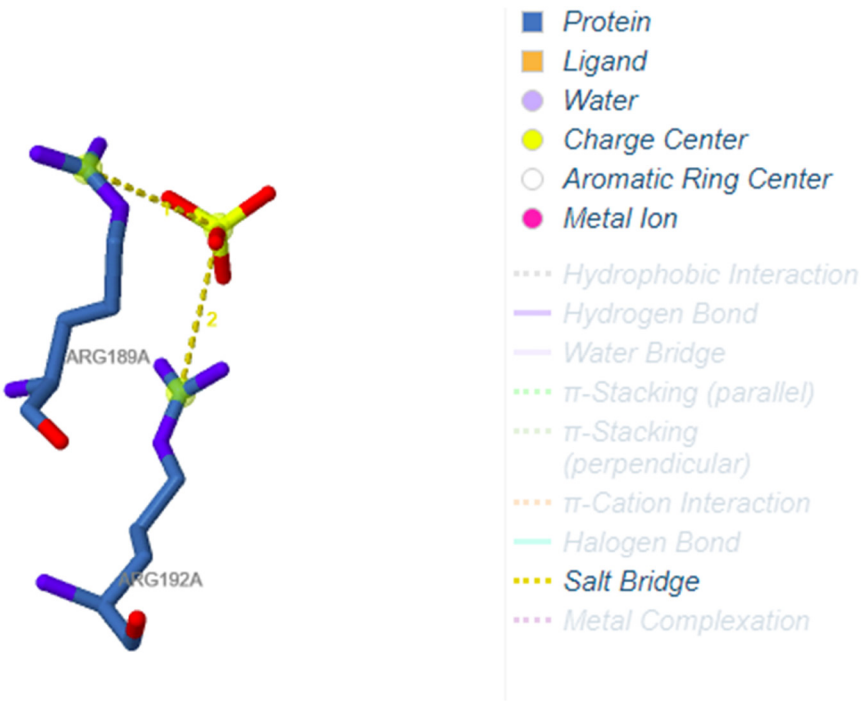


**Figure 6:** Interaction forces prediction by PLIP of the complex of ERK protein with the A + C enriched ZnO NP.

**Table 3:** The prediction of binding free energy of compound and its percentage contributed predicted by MM/PBSA script method of the A + C enriched ZnO NP

| Terms of energy | Value (kJ/mol) | Predicted binding free energy (%) |
|---|---|---|
| Electrostatic force | 14.98 | 70 |
| van der Walls interaction | 10.67 | 12 |
| Solvation (polar) | 120.89 | 0 |
| Solvation (SASA) | 18.90 | 2 |
| Binding energy | −6.78 | 100 |

**Table 4:** Zeta potential of A + C enriched ZnO NP

| Row ID | Predicted zeta potential (mV) | Reliability |
|---|---|---|
| 1 | −40 | Reliable |

does not have any cytotoxic effect and is safe to be administrated as a drug candidate.

## 3.11 Organ's toxicity evaluation

The prediction of the toxicity profile of the A + C enriched ZnO NP shows that the nanoparticle was not toxic as the profile against all toxicity models was inactive. It shows that an LD50 of 910 mg/kg with an average similarity was 20.61 and a prediction accuracy was 12%. Table 5 shows the predicted toxicity profile of the ZNP against the targeted models. Figure 7 shows the toxicity radar chart of the A + C enriched ZnO NP.

## 3.12 Drug likeness and bioactivity analysis

The Lipinski's rule parameters such as miLogP, PSA, a mass range of atoms, range of O, N, OH, and range of rotatable bonds (nrotb) calculated by the Molinspiration tool of A + C enriched ZnO NP shown in Table 6.

## 3.13 ADMET analysis

ADEMT analysis of the A + C enriched ZnO NP is predicted by the admeSAR online server. ADMET profiling shows a molecular weight of 320.54 g/mol, a lipophilicity of −0.99, high water solubility, and good gastrointestinal tract absorption (Table 7).

## 3.14 Molecular dynamic simulations

Molecular dynamic simulation analyses were performed with A + C enriched ZnO NP which shows the best docking score (lowest binding energy with ERK targeted protein). This analysis was done by using the iMods server. The eigon value for the complex is predicted as $8.86293 \times 10^{-5}$.

**Table 5:** The toxicity profile of the A + C enriched ZnO NP against targeted models

| Sr. no | Model | Prediction | Probability |
|---|---|---|---|
| 1 | Hepatotoxicity | Inactive | 0.67 |
| 2 | Carcinogenicity | Inactive | 0.61 |
| 3 | Immunotoxicity | Inactive | 0.99 |
| 4 | Mutagenicity | Inactive | 0.53 |
| 5 | Cytotoxicity | Inactive | 0.71 |
| 6 | Aryl hydrocarbon receptor | Inactive | 0.89 |
| 7 | Androgen receptor (AR) | Inactive | 1.0 |
| 8 | AR-ligand binding domain (AR-LBD) | Inactive | 0.99 |
| 9 | Aromatase | Inactive | 0.99 |
| 10 | Estrogen receptor alpha | Inactive | 0.99 |
| 11 | ER-LBD | Inactive | 0.97 |
| 12 | Peroxisome proliferator activated receptor gamma | Inactive | 0.99 |
| 13 | Nuclear factor (erythroid-derived 2)-like 2/antioxidant responsive element (nrf2/ARE) | Inactive | 0.93 |
| 14 | Heat shock factor response element | Inactive | 0.93 |
| 15 | Mitochondrial membrane potential | Inactive | 0.87 |
| 16 | Phosphoprotein (tumor supressor) p53 | Inactive | 0.94 |
| 17 | ATPase family AAA domain-containing protein 5 (ATAD5) | | 0.99 |

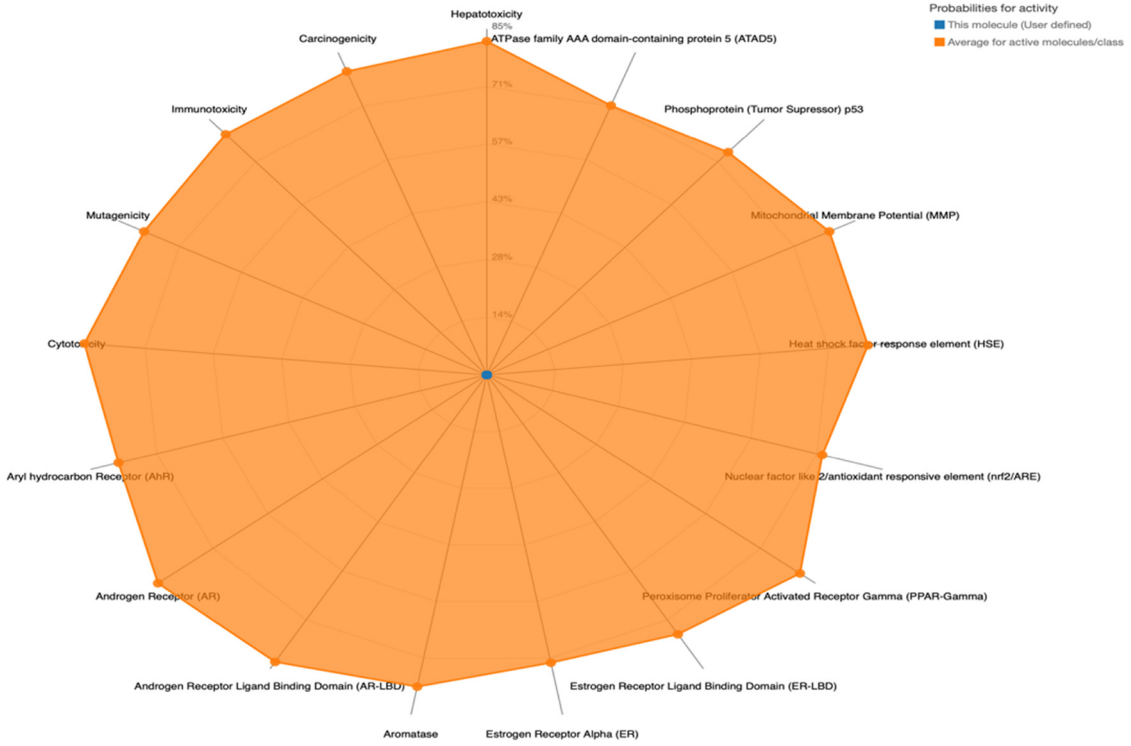


**Figure 7:** Toxicity radar chart analysis of the A + C enriched ZnO NP illustrates the confidence of positive toxicity results compared to the average of its class.

The selected structure of the docking complex with ERK protein shows less deformation at the residue level. Figure 8 explains the details of molecular dynamics simulations of the complex. In Figure 8a, deformability is indicated which shows that there is a low level of deformation at the residue level. Figure 8b shows the b-factor. Figure 8c shows that eigon value is predicted as $8.86293 \times 10^{-5}$. Figure 8d shows the variance which is further elaborated in both green and purple colors. Figure 8e shows the co-variance. Figure 8f shows the elastic network in which the darker grey region indicates the stiffer regions.

## 4 Discussion

The brain is comprised of various cell types, including microglia, which act as the first line of defense in the central nervous system. When activated by infection or injury, microglia may perform the pro-inflammatory and antigen-presenting roles, which causes the production of the pro-inflammatory cytokines [29]. However, excessive activation of microglia cells causes significant CNS destruction as it produces high levels of the neurotoxic cytokine.

**Table 7:** ADMET profiling of + C enriched ZnO NP through admeSAR

| ADMET properties | Parametric values |
|---|---|
| Molecular weight | 320.54 g/mol |
| *A*log *P* (lipophilicity) | −0.99 |
| Blood–brain barrier | Yes |
| P-gp substrate | No |
| Water solubility | −0.951 log *S* |
| Class | Soluble |
| Human oral bioavailability | Yes |

**Table 6:** Validation of parameters of Lipinski's rule

| Sr. no. | Active compound | miLogP | Molecular weight | nON | nOHNH | nrotb |
|---|---|---|---|---|---|---|
| 1 | ZNP | −1.36 | 320.54 | 3 | 5 | 1 |

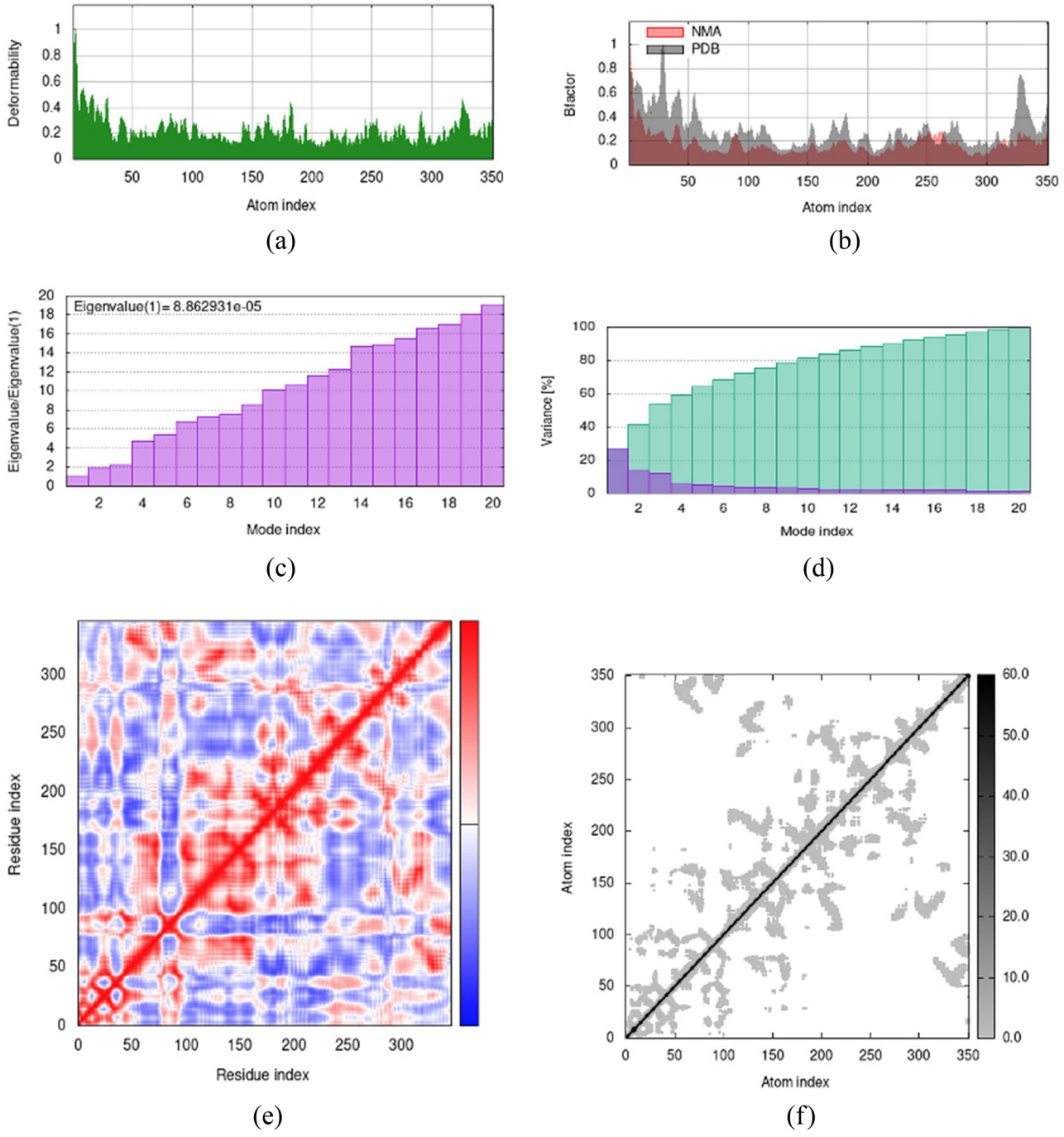


**Figure 8:** The results of molecular dynamic simulations of compound-complex with A + C enriched ZnO NP. (a) Deformability, (b) B-factor, (c) variance (purple color indicates individual variances and green color indicates the cumulative variances), (d) eigon value, (e) co-variance map (correlated [red] anti-correlated [blue] motions), and (f) elastic network (darker grey region indicate stiffer regions).

Additionally, high levels of ROS have been linked to the destruction of cells through lipid peroxidation or cause inflammation [30]. The most severe inflammation is found in the frontal lobes of the brain in autopsies of patients with PAM [31]. Conversely, the posterior parts of the brain, while still hosting trophozoites, show no signs of inflammation and tissue destruction. This proposes that inflammation plays a key role in the tissue damage of the brain observed in PAM patients [32]. Many novel molecules were found against amoeba, 11 molecules were elucidated against *B. mandrillaris*, 9 with activity against *A. castellanii*, and *22* novel molecules were found against *N. fowleri* [33].

In the present study, ZnO NP was taken as a drug candidate against the potential targeted protein ERK, which is involved in the production of the proinflammatory cytokines that cause the destruction of the brain cell in patients of *N. fowleri* infection. Molecular docking analysis shows that zinc oxide exhibits high binding affinity against ERK protein −2.3 kJ/mol of energy. Furthermore, optimization was performed by the addition of two amine groups and one chloride group in the 3D structure of the ZNP. Different studies show that through FTIR analysis it was found that the amine group is present in the nanoparticles that act to modify decomposition temperature, increase solubility, and be used as a capping ligand on nanoparticles [34]. Chlorine is one of the strongest halogens and it increases the stability of the nanoparticles [35]. Through functional group optimization by adding these two groups, the binding affinity increases to −7.8 kJ/mol as both these functional groups increase the stability of the A + C enriched ZnO NP.

Despite efforts to treat the disease, the prognosis remains poor. One of the main reasons is the administration of drugs through intravenous routes, which causes severe side effects like hepatotoxicity and nephrotoxicity, among others, due to drug distribution to non-target tissues [36]. Additionally, the highly selective BBB poses a significant challenge to delivering drugs to the central nervous system, making it difficult to treat amoebic brain infections [37]. The medical significance of pathogenic free-living amoebae and their potential to act as trojan horses in the bacterial world highlight the need for innovative therapies to target them [38]. To this end, there is an ongoing discussion about the use of nanovesicles to deliver innovative and promising therapies against pathogenic free-living amoebae. A + C enriched ZnO NP shows a good profile of ADMET properties as it is water soluble with an *A*log *P* value of less than 4 which is −0.99 means it is lipophilic and shows BBB permeability with no toxicity.

Previously reported nanoparticle-based drugs show cytotoxic effects from the disruption of cellular compartments, immune reactions, and the generation of reactive oxygen species [39]. Orally administered silver NPs have been linked with fecal elimination at high levels, while intraperitoneal or oral administration of gold NPs at high concentrations has been linked with a reduction in red blood cells, body mass index, spleen index, and body weight [40], [41]. In this study, A + C enriched ZnO NP does not show any cytotoxic effect as the prediction of cytotoxicity analysis shows a value of 0.0002, which means that it has no cytotoxic effect on cell lines. A study by Debnath *et al*. identified “corifungin” known as a water-soluble polyene macrodile which shows a high affinity against Naegleria rather than amphotericin B [42]. Another study identified two central nervous system active compounds known as BAY 11-7082 and ebselen show high activity against *N. fowleri* [43]. The prevalence of infections caused by *N. fowleri* is found to increase due to the rise in global temperatures. This poses a significant concern given the growing number of immunocompromised individuals who are at risk of infection. Therefore, developing new strategies to combat infection caused by pathogenic *N. fowleri* is crucial [44].

# 5 Conclusion

Proinflammatory cytokines prompt in the pathogenesis of the *N. fowleri* infection. The ERK causes the activation of the cytokines in response to the *N. fowleri*. The production of these cytokines caused the destruction of the BBB and hyper-inflammation of the immune cells. Recent treatment therapies based on the combinations induce long-term side effects as a high dose of these antibiotics is required causing nephrotoxicity. Nanoparticles retain the efficiency that enables them to cross the BBB. In the current study, ZNP is used as a drug candidate against ERK protein. The enrichment of two amines and one chlorine group enhances its efficiency and efficacy against amoebic infection. Docking analysis shows an increase in the efficiency of the A + C ZnO NP with no organ toxicity or cytotoxicity and it is highly bioavailable as ADMET analysis shows a good profile of solubility. Conclusively, this study will prove as a benchmark in the upcoming arenas of nanotechnology followed by drug discovery.

**Acknowledgments:** The authors greatly acknowledge and express their gratitude to the Researchers Supporting Project number (RSPD2024R568), King Saud University, Riyadh, Saudi Arabia.

**Funding information:** No external funding was received.

**Author contributions:** Conceptualization, M.A., M.N., I.A., N.U., and T.A.; methodology, M.A., M.N., I.A., and N.U.; software, M.A.; validation, A.A.S.; formal analysis, T.A.; investigation, M.A., M.N., S.R., and N.U.; resources, M.A. and A.A.S.; data curation, T.A.; writing – original draft preparation, A.A.K.; writing – review and editing, M.A., M.N., I.A., and N.U.; visualization, F.A. and N.U.; supervision, T.A. and S.N.; project administration, M.A.; funding acquisition, T.A.

**Conflict of interest:** The authors declare no conflict of interest.

**Ethical approval**: The conducted research is not related to either human or animal use.

**Data availability statement:** The datasets generated during and/or analyzed during the current study are available from the corresponding author on reasonable request.

## References


[1] Kemble SK, Lynfield R, DeVries AS, Drehner DM, Pomputius III WF, Beach MJ, et al. Fatal Naegleria fowleri infection acquired in Minnesota: possible expanded range of a deadly thermophilic organism. Clin Infect Dis. 2012;54(6):805–9.

[2] Visvesvara GS. Pathogenic and opportunistic free-living amebae. Man Clin Microbiol. 2015;2387–98.

[3] Retana Moreira L, Zamora Rojas L, Grijalba Murillo M, Molina Castro SE, Abrahams Sandí E. Primary amebic meningoencephalitis related to groundwater in Costa Rica: diagnostic confirmation of three cases and environmental investigation. Pathogens. 2020;9(8):629.

[4] Jahangeer M, Mahmood Z, Munir N, Waraich UA, Tahir IM, Akram M, et al. Naegleria fowleri: Sources of infection, pathophysiology, diagnosis, and management; a review. Clin Exp Pharmacol Physiol. 2020;47(2):199–212.

[5] Rizo-Liendo A, Sifaoui I, Reyes-Batlle M, Chiboub O, Rodríguez-Expósito RL, Bethencourt-Estrella CJ, et al. In vitro activity of statins against Naegleria fowleri. Pathogens. 2019;8(3):122.

[6] Grace E, Asbill S, Virga K. Naegleria fowleri: pathogenesis, diagnosis, and treatment options. Antimicrob Agents Chemother. 2015;59(11):6677–81.

[7] Bellini NK, Santos TM, da Silva MTA, Thiemann OH. The therapeutic strategies against Naegleria fowleri. Exp Parasitol. 2018;187:1–11.

[8] Marciano-Cabral F, Cabral GA. The immune response to Naegleria fowleri amebae and pathogenesis of infection. FEMS Immunol Med Microbiol. 2007;51(2):243–59.

[9] Kim JH, Song AR, Sohn HJ, Lee J, Yoo JK, Kwon D, et al. IL-1β and IL-6 activate inflammatory responses of astrocytes against N aegleria fowleri infection via the modulation of MAPK s and AP-1. Parasite Immunol. 2013;35(3–4):120–8.

[10] Visvesvara GS. Infections with free-living amebae. Handb Clin Neurol. 2013;114:153–68.

[11] Jamerson M, Schmoyer JA, Park J, Marciano-Cabral F, Cabral GA. Identification of Naegleria fowleri proteins linked to primary amoebic meningoencephalitis. Microbiology. 2017;163(3):322–32.

[12] Mungroo MR, Anwar A, Khan NA, Siddiqui R. Brain-eating amoebae infection: Challenges and opportunities in chemotherapy. Mini Rev Med Chem. 2019;19(12):980–7.

[13] Maciver SK, Piñero JE, Lorenzo-Morales J. Is Naegleria fowleri an emerging parasite? Trends Parasitol. 2020;36(1):19–28.

[14] Barani M, Mukhtar M, Rahdar A, Sargazi G, Thysiadou A, Kyzas GZ. Progress in the application of nanoparticles and graphene as drug carriers and on the diagnosis of brain infections. Molecules. 2021;26(1):186.

[15] Gilpin W. PyPDB: a Python API for the protein data bank. Bioinformatics. 2016;32(1):159–60.

[16] Giannetti M, Mazzuca C, Ripani G, Palleschi A. Inspection on the mechanism of SARS-CoV-2 inhibition by penciclovir: A molecular dynamic study. Molecules. 2023;28(1):191.

[17] Kim S, Thiessen PA, Bolton EE, Chen J, Fu G, Gindulyte A, et al. PubChem substance and compound databases. Nucleic Acids Res. 2016;44(D1):D1202–D13.

[18] Chandel V, Srivastava M, Srivastava A, Asthana S, Kumar D. In-silico interactions of active Phytochemicals with c-MYC EGFR and ERBB2 oncoproteins. Chem Biol Lett. 2020;7(1):47–54.

[19] Mali SN, Chaudhari HK. Computational studies on imidazo [1, 2-a] pyridine-3-carboxamide analogues as antimycobacterial agents: Common pharmacophore generation, atom-based 3D-QSAR, molecular dynamics simulation, QikProp, molecular docking and prime MMGBSA approaches. Open Pharm Sci J. 2018;5:1.

[20] Bernard M, Rué O, Mariadassou M, Pascal G. FROGS: a powerful tool to analyse the diversity of fungi with special management of internal transcribed spacers. Brief Bioinforma. 2021;22(6):bbab318.

[21] Naveed M, Shabbir MA, Ain N-u, Javed K, Mahmood S, Aziz T, et al. Chain-engineering-based de novo drug design against MPXVgp169 virulent protein of monkeypox virus: A molecular modification approach. Bioengineering. 2023;10(1):11.

[22] Thompson DC, Humblet C, Joseph-McCarthy D. Investigation of MM-PBSA rescoring of docking poses. J Chem Inf modeling. 2008;48(5):1081–91.

[23] Varsou DD, Afantitis A, Tsoumanis A, Papadiamantis A, Valsami-Jones E, Lynch I, et al. Zeta-potential read-across model utilizing nanodescriptors extracted via the nanoxtract image analysis tool available on the enalos nanoinformatics cloud platform. Small. 2020;16(21):1906588.

[24] Papadiamantis AG, Jänes J, Voyiatzis E, Sikk L, Burk J, Burk P, et al. Predicting cytotoxicity of metal oxide nanoparticles using Isalos analytics platform. Nanomaterials. 2020;10(10):2017.

[25] Banerjee P, Eckert AO, Schrey AK, Preissner R. ProTox-II: a webserver for the prediction of toxicity of chemicals. Nucleic Acids Res. 2018;46(W1):W257–W63.

[26] Shaheen U, Akka J, Hinore JS, Girdhar A, Bandaru S, Sumithnath TG, et al. Computer aided identification of sodium channel blockers in the clinical treatment of epilepsy using molecular docking tools. Bioinformation. 2015;11(3):131.

[27] Kumar S, Patel R. COVID moonshot computer-aided drug design of SARS-CoV-2 oral antivirals. 2021

[28] Naveed M, Makhdoom SI, Ali U, Jabeen K, Aziz T, Khan AA, et al. Immunoinformatics approach to design multi-epitope-based vaccine against machupo virus taking viral nucleocapsid as a potential candidate. Vaccines. 2022;10(10):1732.

[29] Boche D, Perry V, Nicoll J. Activation patterns of microglia and their identification in the human brain. Neuropathol Appl Neurobiol. 2013;39(1):3–18.

[30] Martínez-Castillo M, Santos-Argumedo L, Galván-Moroyoqui JM, Serrano-Luna J, Shibayama M. Toll-like receptors participate in Naegleria fowleri recognition. Parasitol Res. 2018;117:75–87.

[31] Hall ED, Wang JA, Bosken JM, Singh IN. Lipid peroxidation in brain or spinal cord mitochondria after injury. J Bioenerg Biomembr. 2016;48:169–74.

[32] Cervantes-Sandoval I, Serrano-Luna J de J, Garcia-Latorre E, Tsutsumi V, Shibayama M. Characterization of brain inflammation during primary amoebic meningoencephalitis. [Research Support, Non-US Gov't]. Parasitol Int. 2008;57:307–13.

[33] Rice CA, Troth EV, Russell AC, Kyle DE. Discovery of anti-amoebic inhibitors from screening the MMV pandemic response box on

Balamuthia mandrillaris, Naegleria fowleri, and Acanthamoeba castellanii. Pathogens. 2020;9(6):476.
[34] Hsiao IL, Fritsch-Decker S, Leidner A, Al-Rawi M, Hug V, Diabaté S, et al. Biocompatibility of amine-functionalized silica nanoparticles: the role of surface coverage. Small. 2019;15(10):1805400.
[35] Chen Y, Zhang T, Chai D, Ye H, Tang S, Wang P, et al. Enhancing the NaCl/Na2SO4 separation selectivity and chlorine resistance of nanofiltration membranes by incorporating novel designed starch nanoparticles. Appl Surf Sci. 2022;604:154417.
[36] Rajendran K, Anwar A, Khan NA, Siddiqui R. Brain-eating amoebae: Silver nanoparticle conjugation enhanced efficacy of anti-amoebic drugs against Naegleria fowleri. ACS Chem Neurosci. 2017;8(12):2626–30.
[37] Cárdenas-Zúñiga R, Silva-Olivares A, Villalba-Magdaleno JDA, Sánchez-Monroy V, Serrano-Luna J, Shibayama M. Amphotericin B induces apoptosis-like programmed cell death in Naegleria fowleri and Naegleria gruberi. Microbiology. 2017;163(7):940–9.
[38] Heggie TW, Küpper T. Surviving Naegleria fowleri infections: a successful case report and novel therapeutic approach. Travel Med Infect Dis. 2017;16:49–51.
[39] Sharma G, Kalra SK, Tejan N, Ghoshal U. Nanoparticles based therapeutic efficacy against Acanthamoeba: Updates and future prospect. Exp Parasitol. 2020;218:108008.
[40] Bergin IL, Wilding LA, Morishita M, Walacavage K, Ault AP, Axson JL, et al. Effects of particle size and coating on toxicologic parameters, fecal elimination kinetics and tissue distribution of acutely ingested silver nanoparticles in a mouse model. Nanotoxicology. 2016;10(3):352–60.
[41] Kasra KR, Hojati V, Shiravi A. Zinc oxide nanoparticles absorption rate in the heart tissue of female mice. 2015;8(2):193–8.
[42] Debnath A, Tunac JB, Galindo-Gómez S, Silva-Olivares A, Shibayama M, McKerrow JH. Corifungin, a new drug lead against Naegleria, identified from a high-throughput screen. Antimicrob Agents Chemother. 2012;56(11):5450–7.
[43] Debnath A, Nelson AT, Silva-Olivares A, Shibayama M, Siegel D, McKerrow JH. In vitro efficacy of ebselen and BAY 11-7082 against Naegleria fowleri. Front Microbiol. 2018;9:414.
[44] Bhosale NK, Parija SC. Balamuthia mandrillaris: An opportunistic, free-living ameba–An updated review. Tropical. Parasitology. 2021;11(2):78.